

# Semiclassical Monte Carlo model for in-plane transport of spin-polarized electrons in III–V heterostructures

Semion Saikin

*Center for Quantum Device Technology, Department of Electrical and Computer Engineering and Department of Physics, Clarkson University, Potsdam, New York 13699-5720 and Department of Physics, Kazan State University, Kazan, Russian Federation*

Min Shen and Ming-C. Cheng

*Center for Quantum Device Technology, Department of Electrical and Computer Engineering, Clarkson University, Potsdam, New York 13699-5720*

Vladimir Privman<sup>a)</sup>

*Center for Quantum Device Technology, Department of Electrical and Computer Engineering and Department of Physics, Clarkson University, Potsdam, New York 13699-5720*

Received 2 January 2003; accepted 16 May 2003

We study the in-plane transport of spin-polarized electrons in III–V semiconductor quantum wells. The spin dynamics is controlled by the spin-orbit interaction, which arises due to the bulk crystalline-structure asymmetry and quantum-well inversion asymmetry. This interaction, owing to its momentum dependence, causes rotation of the spin-polarization vector, and also produces effective spin dephasing. The density matrix approach is used to describe the evolution of the electron spin polarization, while the spatial motion of the electrons is treated semiclassically. Monte Carlo simulations have been carried out for temperatures in the range 77–300 K. © 2003 American Institute of Physics. DOI: 10.1063/1.1589581

## I. INTRODUCTION

Promising applications of spintronics for device structures<sup>1–5</sup> have stimulated much interest in spin-polarized transport. Many devices utilizing spin-dependent phenomena have been proposed recently.<sup>6–14</sup> At the present time, there are numerous difficulties with control of spin-polarized current. Recent experimental advances<sup>2</sup> have allowed generation of spin polarization of conduction electrons in bulk semiconductors and in two-dimensional semiconductor structures. At room temperatures, spin polarization can be maintained for up to 1–2 ns.

Experimental investigations of spin-polarized transport in semiconductors can be divided into three main areas: injection and detection of spin-polarized current, spin relaxation of conduction electrons, and coherent spin dynamics.

Among a few methods to create electron spin polarization in semiconductors,<sup>15–18</sup> the electrical spin injection from magnetic contacts<sup>17,18</sup> is the most promising. However, the main difficulty of this approach has been in the correct band matching at the interface of magnetic material–semiconductor.<sup>19,20</sup> Also, the all-electrical experiments on the detection of spin injection are complicated by additional spin-independent effects, which are difficult to separate from spin-dependent phenomena.<sup>21</sup> Thus, the recently reported values of the experimentally achieved spin polarization at room temperature have varied from 1%–2% Ref. 22 up to 30%–35%.<sup>23,24</sup> At low temperatures,  $T$  4.2 K, the polarization of the electrons injected from mag-

netic semiconductor contacts is appreciably higher and reaches the values of 50%–80%.<sup>25,26</sup>

The optical electron spin-polarization and detection methods<sup>16</sup> are, perhaps, less applicable in the device design, but they have been very useful in investigations of electron spin dynamics, due to high efficiency of spin polarization at room temperature more than 50% and high sensitivity of measurement. Spin relaxation in semiconductor heterostructures has been studied extensively by the methods of ultrafast spin-sensitive spectroscopy.<sup>27–31</sup> At room temperature, the observed spin-relaxation time varies widely, from less than 1 ps for structures with a large spin-orbit interaction,<sup>27</sup> up to 1 ns Ref. 28 for GaAs/AlGaAs quantum wells QWs with a suppressed Dyakonov–Perel relaxation mechanism.<sup>32</sup>

The spin-lattice relaxation of conduction electrons at high temperatures is dominated by several mechanisms arising from spin-orbit coupling. Their relative strength is determined by many different factors, some of which are established during the growth of the heterostructure and cannot be well controlled. While for  $n$ -doped GaAs/AlGaAs QWs with 001 growth orientation the main relaxation mechanism at room temperature is Dyakonov–Perel,<sup>30</sup> spin relaxation in narrow band gap InGaAs/InP, InGaAs/InAlAs heterostructures has no single explanation due to more complicated spin-orbit interactions.<sup>29,31</sup>

Generally, the conduction electron spin dynamics is controlled by external magnetic field, local magnetic fields produced by magnetic impurities and nuclei, and spin orbit interactions. In comparison with the electron spin-transport model for ferromagnetic structures, which can be described within the two-current model,<sup>33</sup> for nonmagnetic bulk semiconductors and semiconductor heterostructures the spin-orbit

<sup>a)</sup> Electronic mail: privman@clarkson.edu

term is significant. This effect has been investigated by analyzing the Shubnikov–de Haas oscillations of the magnetoresistance in moderate magnetic fields<sup>34,35</sup> and studying weak antilocalization in nearly zero fields.<sup>36–38</sup> The tuning of the spin-orbit coupling constant by the gate voltage, which has been proposed for current modulation in the spin field-effect transistor FET,<sup>6</sup> was demonstrated recently for InGaAs/InAlAs asymmetric QWs.<sup>35,39</sup>

In the low-temperature and low-voltage regime, the value of the spin mean-free path in bulk GaAs can reach few  $\mu\text{m}$ ,<sup>40,41</sup> which is much larger than industrially achievable device sizes.<sup>42</sup> The above overview of selected promising experimental results for spintronics device development, suggests that it is timely to develop device-modeling approaches incorporating spin polarization effects.

For low temperatures and low applied voltage, the single-particle ballistic models have been utilized.<sup>13,43,44</sup> Many of the existing semiclassical models have been developed along the lines of the earlier approach used for ferromagnetic layered structures.<sup>33</sup> They are primarily of the drift–diffusion category, where the spin-up and spin-down electrons are described by charge- and spin-density conservation equations.<sup>45–47</sup> These models ignore quantum coherence effects of possible superposition of the spin-up and spin-down states, which can be described in terms of the polarization vector.<sup>48</sup> The range of applicability for such models is limited by many factors—electric field, device size, etc.—when nonlinear effects become important.<sup>20,41</sup> However, the derived drift–diffusion models<sup>45–47</sup> have been useful in addressing general problems of spin-polarized transport. For instance, a self-consistent solution of the Poisson equation and four nonlinear continuity equations<sup>49</sup> allows inclusion of inhomogeneous electric and magnetic fields, consideration of arbitrary doping profile, high applied bias and other effects. For hot-electron spin-polarized transport, the coupled Boltzmann equations with only spin-up and spin-down states,<sup>50</sup> or additionally including superimposed up–down states,<sup>51,52</sup> have been considered.

Spin relaxation of conduction electrons and their spatial motion cannot be separated exactly. However, in some drift–diffusion approximations, it can be shown that spin polarization of the electron gas decays exponentially in time in accordance with the spin-relaxation Bloch equations<sup>53,54</sup> with characteristic times  $T_1$  and  $T_2$ . It is reasonable to assume, in analogy with the energy and momentum relaxation times<sup>55</sup> in energy-balance or hydrodynamic models for semiconductor devices, that these parameters will depend on the electron temperature,  $T_e$ , and, possibly, some other variables.<sup>56</sup> Monte Carlo simulation including the electron spin state<sup>57–59</sup> can be useful for spin-dynamics modeling in the nonlinear regime and extraction of such parameters. In this work, we utilize the Monte Carlo approach to simulate spin polarized transport in asymmetric QWs for intermediate values of the electric field ( $2\text{--}4\text{ kV/cm}$ ), for temperature  $T$   $77\text{--}300\text{ K}$ .

## II. SEMICLASSICAL DENSITY MATRIX APPROACH TO SPIN-POLARIZED ELECTRON TRANSPORT

The Monte Carlo approach to the Boltzmann equation for nonstationary electron transport has been widely used for modeling of submicrometer and deep-submicrometer devices.<sup>60,61</sup> Here, we incorporate the description of the electron spin dynamics in a standard semiclassical Monte Carlo formalism.<sup>60,61</sup> The effective single-electron Hamiltonian with the spin-orbit SO interaction term is

$$H = H_0 + H_{SO}(\mathbf{k}). \quad (1)$$

In the absence of external and local magnetic fields, the electron magnetic interaction is only owing to the spin-orbit term  $H_{SO}(\mathbf{k})$  in Eq. 1.  $H_0$  is the self-consistent single electron Hamiltonian in the Hartree approximation, including also interactions with phonons and static imperfections. Inside the QW, this can be written as

$$H_0 = \frac{\hbar^2 k^2}{2m^*} + e \mathbf{r} \cdot \mathbf{E}_{\text{ext}} + H_{e\text{-ph}} + H_{\text{ph}} + V_{\text{imp}}. \quad (2)$$

In the semiclassical treatment,<sup>60</sup> the operator  $\mathbf{k}$  is considered as the momentum vector in the  $xy$  plane of the QW, while the motion in the  $z$  direction is quantized. We consider here a structure grown in the  $[0, 0, 1]$  direction, and assume that the in-channel electric field is applied along the  $x$  crystallographic axis. These assumptions allow us to specify the form of spin-orbit interaction term, Eq. 1.<sup>32</sup> The coordinate axes are chosen parallel to the crystallographic directions. The screening factor  $\mathbf{r}$  accounts for the electron–electron interactions. It is determined by the appropriate Poisson equation.<sup>62</sup> The term  $V_{\text{imp}}$  describes ionized nonmagnetic impurities, QW roughness, and other static imperfections of its structure. The terms labeled “ $e\text{-ph}$ ” and “ $\text{ph}$ ” represent the electron–phonon interactions and the phonon mode Hamiltonian. The main contributions to the spin-orbit interaction in an asymmetric III–V semiconductor QW structure are due to the Dresselhaus mechanism,<sup>32,63</sup>

$$H_D = \frac{\hbar}{2} (k_z^2 k_y - k_y k_x), \quad (3)$$

and the Rashba mechanism,<sup>64</sup>

$$H_R = \alpha (k_y k_x - k_x k_y). \quad (4)$$

Equation 3 as written, is only applicable for narrow QWs, such that  $k_x, k_y \ll k_z$ . For submicrometer devices with smooth potential, in the considered temperature regime ( $T$   $77\text{--}300\text{ K}$ ), we assume that the spatial electron transport is semiclassical and can be described by the Boltzmann equation.<sup>62</sup> The electrons follow classical localized trajectories between the scattering events. The scattering rates are given by the Fermi Golden Rule, and the scattering events, are instantaneous. We also assume that the Elliott–Yafet spin-scattering mechanism<sup>65</sup> is inefficient, i.e., that there are no electron spin flips accompanying momentum scattering. The backreaction of the electron spin evolution on the spatial motion is negligible owing to the small value of the electron momentum-state splitting due to the spin-orbit interaction in comparison with its average momentum.

TABLE I. Parameters of the confining potential, and the spin-orbit interaction coupling constants.

$d$ nm	$E_c$ eV	$n$ (cm <sup>-2</sup> )	$E_1$ eV	$k_z^2$ <sup>1/2</sup> (nm <sup>-1</sup> )	eV Å	(eV Å <sup>3</sup> )
20	0.56	1 · 10 <sup>12</sup>	0.20	0.21	0.074	32.20

In Monte Carlo simulations, it is assumed that electrons propagate with constant velocity during the time  $t$ , which is the smaller of the grid time step and the time interval either left to the next scattering or from scattering to the next sampling. We term such a motion free flight. The propagation velocity of an electron in free flight was taken as the average value of the velocity of an electron moving with constant acceleration during  $t$ . Among many different scattering mechanisms,<sup>66</sup> our Monte Carlo simulation has included charged impurity and phonon scatterings. The phonon bath in Eq. 2 is assumed to remain in thermal equilibrium with the constant lattice temperature  $T$  at all times. In the semiclassical Monte Carlo, the temperature is incorporated in the electron-phonon scattering rates.<sup>60,61</sup> Details of the Monte Carlo simulation model are described elsewhere.<sup>67</sup>

For the description of the electron spin, we use the standard spin-density matrix,<sup>68</sup>

$$t \begin{pmatrix} \uparrow\uparrow & \uparrow\downarrow \\ \downarrow\uparrow & \downarrow\downarrow \end{pmatrix} t, \tag{5}$$

which is associated with the spin-polarization vector as  $S(t) = \text{Tr}(\sigma(t))$ , where  $(\sigma_x, \sigma_y, \sigma_z)$  are Pauli matrixes.<sup>68</sup> For each free flight time interval,  $t$ , the spin-density matrix evolves according to

$$t \rightarrow t e^{iH_{SO} t/ \hbar} t e^{iH_{SO} t/ \hbar}. \tag{6}$$

This is equivalent to rotation of the spin-polarization vector about the effective magnetic field determined by the direction of the electron momentum. The exponential operators in Eq. 6 can be written as (2 · 2) scattering matrices,

$$e^{iH_{SO} t/ \hbar} = \begin{pmatrix} \cos \theta & i \sin \theta \\ i \sin \theta & \cos \theta \end{pmatrix}, \tag{7}$$

and Hermitean conjugate of Eq. 7 for the operator  $e^{-iH_{SO} t/ \hbar}$ . Here,  $\theta$  is determined by the spin-orbit interaction terms, Eqs. 3 and 4 :

$$\theta = \frac{1}{\hbar} (k_y^2 k_x - k_z^2 k_x + i k_x k_y - k_z^2 k_y). \tag{8}$$

During the free flight, the spin dynamics of a single electron spin is coherent; see Eq. 6. However, stochastic momentum fluctuations during the scattering events, produce distribution of spin states, thus causing effective dephasing at times  $t > 0$ . The spin polarization,  $S$ , of the current can be obtained by averaging  $S$  over all the electrons in a small volume  $dv$ , which is located at position  $\mathbf{r}$ , at time  $t$ . The absolute value of the average spin-polarization vector is in the range  $0 \leq S \leq 1$ . If  $S = 1$ , the electric current is completely spin polarized. The components  $S_x, S_y, S_z$  define the orientation of the spin polarization, and evolution of the spin polariza-

tion vector may be viewed as coherent motion rotation accompanied by depolarization reduction of magnitude.

### III. MODEL AND SIMULATION RESULTS

We have utilized the model of spin-polarized current, described in the preceding section, in simulation of electron transport in a single QW. Here, we use asymmetric QW architecture in the one-subband approximation, which is a simplified model of  $\text{In}_{0.52}\text{Al}_{0.48}\text{As}/\text{In}_{0.53}\text{Ga}_{0.47}\text{As}/\text{In}_{0.52}\text{Al}_{0.48}\text{As}$  heterostructures used in experiments probing the spin-orbit coupling effects.<sup>35</sup> Theoretically estimated values of the spin-orbit coupling constants vary for different models and band parameters, within 30%–50% for example, see Refs. 69–71 for the Dresselhaus coupling constants. For our simulations, the Rashba coupling constant was taken from Ref. 35, while for the Dresselhaus coupling constant we took a typical representative value, close to that experimentally measured<sup>69</sup> for GaAs. A value approximately twice as large would be obtained if we used a linear extrapolation between this GaAs experimental value and theoretical estimation<sup>70</sup> for bulk InAs. Parameters of the confining potential and spin-orbit interaction are given in Table I; see Fig. 1 for the potential shape.

We denote by  $n$  the equilibrium electron density in the channel. The ratio of the expectation values for the Dresselhaus and Rashba energy terms, Eqs. 3 and 4, is  $E_R/E_D = 5.3$ , which means that the Rashba term is dominant both for the coherent polarization-rotation dynamics and for depolarization.

In our simulations, the device length was taken  $l = 0.55 \mu\text{m}$ . The grid time step was  $t_{\text{grid}} = 1 \text{ fs}$ . The material and scattering-rate parameters were taken from the literature.<sup>66</sup> To achieve the steady-state transport regime, we ran the simulation program for 20 000 time steps, and collected data only during the last 2000 time steps. The simulations were carried out for temperatures  $T = 77\text{--}300 \text{ K}$  and applied drain-source voltage  $V_{\text{DS}} = 0.1\text{--}0.25 \text{ V}$ , which creates the in-channel electric field of the order of 2–4.5 kV/cm.

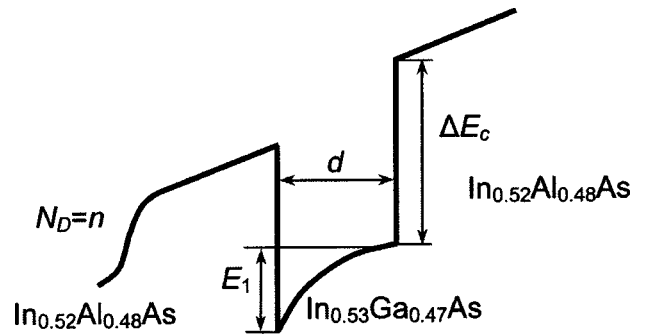


FIG. 1. Model of the confining potential in the asymmetric  $\text{In}_{0.52}\text{Al}_{0.48}\text{As}/\text{In}_{0.53}\text{Ga}_{0.47}\text{As}/\text{In}_{0.52}\text{Al}_{0.48}\text{As}$  quantum well.

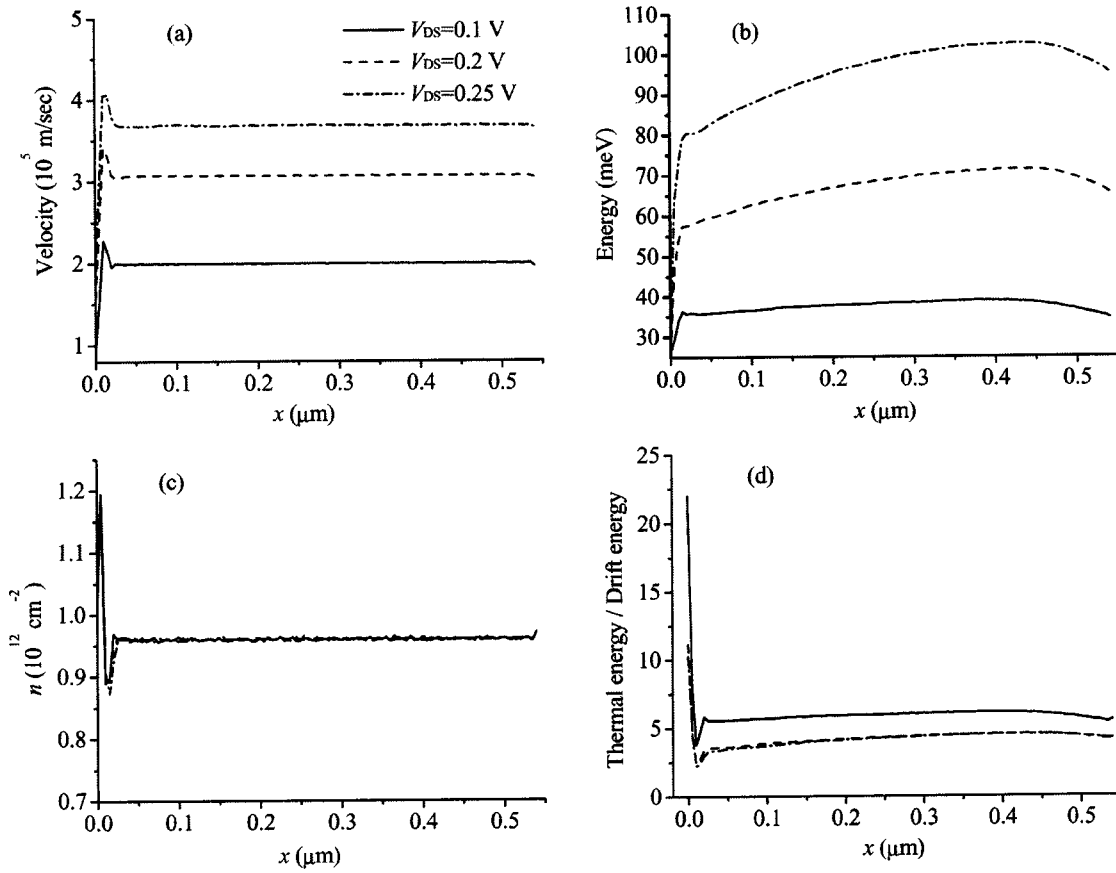


FIG. 2. Electron transport parameters: a drift velocity, b average energy, c electron concentration in the channel, and d electron thermal energy, as compared to their drift energy, as functions of  $x$ , at  $T = 300$  K,  $V_{DS} = 0.1$ – $0.25$  V.

The following boundary conditions were assumed: thermalized electrons were injected at the left boundary, with 100% injected spin polarization, and drained at the right boundary, with any spin polarization.

In the simulated device structure, the electron transport is nonequilibrium; see Fig. 2. Evident velocity overshoot and other sharp features are observed due to sudden increase in the electric field near the injection boundary at all applied voltages. The electron average energy in the two-dimensional quantum well includes the drift and thermal energies,

$$E = \frac{1}{2} m^* \mathbf{v}^2 + kT_e. \quad (9)$$

Near the boundary at  $x = 0$ , where electrons are just injected, the thermal energy  $kT_e$  is dominant.

Due to finite scattering rate ( $\sim 10^{13} \text{ s}^{-1}$ ), ballistic motion is observed in Fig. 2 a for distances as small as  $0.01 \mu\text{m}$ , where average velocity increases considerably. This results in a sudden decrease in the ratio between the thermal and drift energies, as seen in Fig. 2 d, and leads to an abrupt increase in the average energy, shown in Fig. 2 b. After the ballistic region, electrons suffer strong scattering that randomizes momentum and gives rise to velocity overshoot. In order to maintain the current continuity, the electron concentration markedly drops at the location of the velocity overshoot; see Fig. 2 c.

We calculate the evolution of the current spin polarization for three injected polarizations: along the positive  $x$ ,  $y$ , and  $z$  directions. The corresponding injected single-electron density matrixes are

$$\begin{aligned} x \quad & \frac{1}{2} \begin{pmatrix} 1 & 1 & 1 \\ 1 & 1 & 1 \\ 1 & 1 & 1 \end{pmatrix}, & y \quad & \frac{1}{2} \begin{pmatrix} 1 & 1 & i \\ i & 1 & 1 \\ 1 & 1 & 1 \end{pmatrix}, \\ z \quad & \begin{pmatrix} 1 & 0 \\ 0 & 0 \end{pmatrix}. \end{aligned} \quad (10)$$

Due to the symmetry of the Rashba spin-orbit interaction term, Eq. 4, the spin polarization of the electrons, which propagate collectively in the  $x$  direction, will rotate about the  $y$  axis. This is shown in Fig. 3, where from now on we omit the angular brackets that indicate averaging. The Dresselhaus term, Eq. 3, causes rotation about the  $x$  axis. Small admixture of the latter mechanism leads to variation of the  $y$  projection of the spin polarization, see Figs. 3 a and 3 c, and of the  $x$  and  $z$  projections, see Fig. 3 b, depending on the injected spin orientation.

The observed decay of the spin polarization occurs by dephasing owing to the electron momentum scattering events. Random momentum fluctuations, which are described by the electron thermal energy, produce an effective depolarization mechanism. The initial spin polarization drop in Fig. 3 can be attributed to the effect of high electron

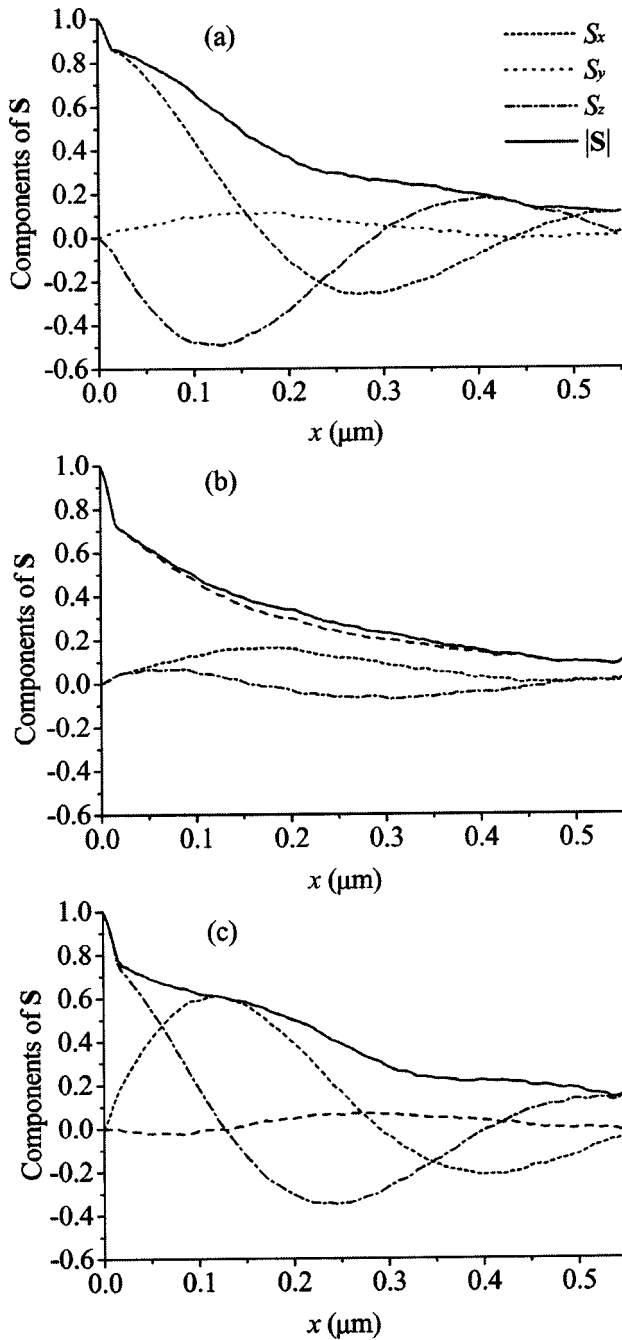


FIG. 3. Evolution of the electron spin polarization  $\mathbf{S}$ , for  $V_{DS} = 0.1$  V, at room temperature (300 K), for three different injected orientations of the spin polarization, along the positive a)  $x$ , b)  $y$ , and c)  $z$  axes.

thermal energy in comparison with the drift energy, see Fig. 2 d). This can be clearly observed in Fig. 4 c), where the drop of the spin polarization near  $x = 0$  is smaller for lower temperatures. Moreover, Fig. 4 b) shows that this drop is evidently less pronounced at higher applied voltage that enhances the drift velocity and relatively weakens the effect of the random momentum fluctuations. This drop could also be an artifact of the free flight assumption for regimes with strong acceleration.

The depolarization rate in our model is asymmetric in the spin orientation. For example, the term proportional to  $k_y \cdot x$  in the Rashba spin-orbit interaction, Eq. 4, produces

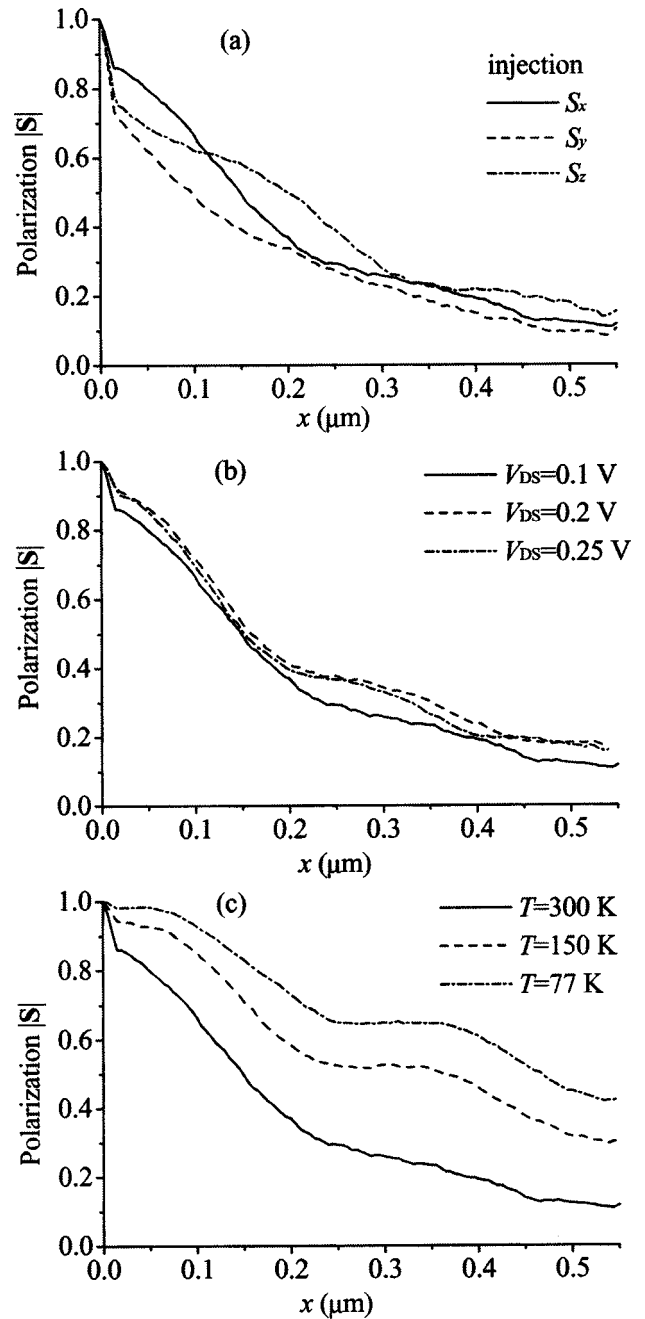


FIG. 4. Spin depolarization effect for a) different orientations of the injected polarization,  $T = 300$  K,  $V_{DS} = 0.1$  V; b) different values of applied voltage,  $T = 300$  K, injected polarization  $S_x = 1$ ; c) different temperatures, injected polarization  $S_x = 1$ ,  $V_{DS} = 0.1$  V.

depolarization of the  $S_y$  and  $S_z$  components, due to the fluctuating  $k_y$ ,<sup>6</sup> but does not influence the  $S_x$  component of the spin polarization. The depolarization rate owing to the Rashba interaction is suppressed for an  $S_x$ -polarized current in comparison with  $S_y$  and  $S_z$ . This effect can be seen in Fig. 4 a).

As shown in Fig. 4 b), the spin polarization at room temperature is not sensitive to the applied voltage in the investigated regime. Higher applied voltage, which leads to considerably larger drift velocity, only slightly increases the spin-dephasing length. Change of the spin polarization at higher applied voltage is minimized by the increase in the

mean energy that in turn increases the scattering probability. For lower temperatures, this quasibalance apparently breaks down. Sufficient reduction of the temperature can suppress the electron–phonon scattering mechanism to yield longer spin mean-free path. The temperature effect on the spin polarization in the range  $T = 77\text{--}300\text{ K}$  is shown in Fig. 4 c . The calculated values of the spin mean free path at  $V_{DS} = 0.1\text{ V}$  are  $L_x = 0.2\text{ }\mu\text{m}$  and  $L_x = 0.55\text{ }\mu\text{m}$ , for  $T = 300\text{ K}$  and  $T = 77\text{ K}$ , respectively. These values are significantly smaller than those obtained for bulk GaAs in the low-temperature ( $T = 9\text{ K}$ ) regime,<sup>40,41</sup>  $L_x = 4\text{ }\mu\text{m}$ , which could be attributed to stronger scattering.

#### IV. DISCUSSION

The simulation model developed in this article includes the linear terms of the spin-orbit coupling. The terms cubic in the components of the momentum  $\mathbf{k}$  in the Dresselhaus spin-orbit interaction,<sup>63</sup> and external magnetic field, can produce additional spin dephasing.<sup>72</sup> The Elliot–Yafet spin-scattering mechanism can be efficient in narrow-gap heterostructures. It can be included in our simulation model as an additional spin-evolution process at momentum scattering events.

The single subband approximation can be questioned for considered values of the applied voltage. For the confining potential used in the simulation, the estimated splitting between the ground and first-excited subbands is  $E_{12} = 60\text{--}70\text{ meV}$ . The intersubband scattering becomes effective at kinetic energies near  $E_{12} \approx 35\text{ meV}$ , when optical phonon absorption becomes possible. Strong scattering sets in when the electron energy is above  $E_{12} \approx 100\text{ meV}$ , and emission of optical phonons becomes possible. According to Fig. 2 b , the average electron energy exceeds the minimum value for the intersubband scattering for  $V_{DS} = 0.1\text{ V}$ . Up to the energy value of  $100\text{ meV}$ , intersubband scattering rate is much less than intrasubband scattering rate,<sup>62</sup> and we can assume that the single subband approximation gives a qualitatively correct description up to the  $V_{DS} = 0.25\text{ V}$ . For low temperatures, the average energy is reduced due to the condition of initial thermalization, Fig. 5 a , but, on the other hand, the electron-phonon scattering is suppressed, resulting in the energy increase, see Fig. 5 b . In comparison with the data shown in Fig. 2 b , the maximum value of the average electron energy for  $V_{DS} = 0.2\text{ V}$  is nearly the same. As a result, it is difficult to extend the validity of the single subband model for  $V_D = 0.2\text{ V}$  by reducing the temperature. For different subbands, the spin-orbit coupling constants are different, and it is likely that the spin dephasing will be even stronger if the intersubband scattering is incorporated.

#### V. SUMMARY

We have developed a semiclassical Monte Carlo model incorporating the linear terms of the Dresselhaus and Rashba spin-orbit coupling mechanisms for spin-polarized electron transport in III–V heterostructures. This approach can be used for simulation of nonequilibrium spin-dependent phenomena in spintronics devices. We reported results for dy-

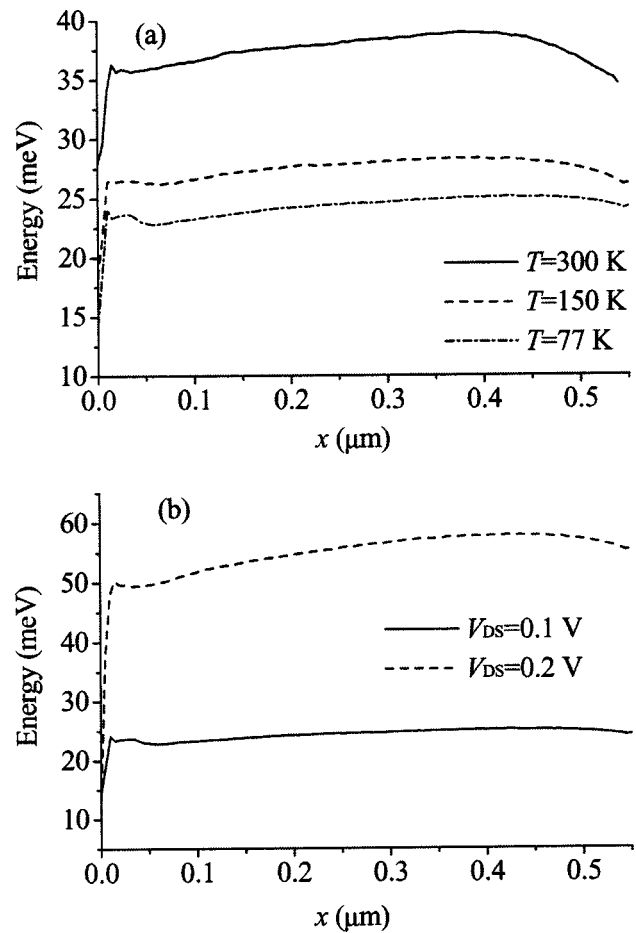


FIG. 5. Average electron energy for different values of the a temperature at  $V_{DS} = 0.1\text{ V}$ ; b applied voltage at  $T = 77\text{ K}$ .

namics of the spin polarization in a single quantum well at several temperatures and intermediate,  $2\text{--}4\text{ kV/cm}$ , electric fields. The estimated spin-depolarization length is of the order of  $0.2\text{ }\mu\text{m}$ . The present-day semiconductor device component dimensions are comparable or smaller. Thus, our results confirm that spintronic effects can be observed and controlled in properly designed modern semiconductor structures.

#### ACKNOWLEDGMENTS

The authors thank Professors A. Shik and I. D. Vagner for helpful discussions. This research was supported by the National Security Agency and Advanced Research and Development Activity under Army Research Office Contract No. DAAD-19-02-1-0035, and by the National Science Foundation, Grant Nos. DMR-0121146 and ECS-0102500.

<sup>1</sup>S. Das Sarma, J. Fabian, X. Hu, and I. Zutic, *IEEE Trans. Magn.* **36**, 2821 (2000).

<sup>2</sup>S. A. Wolf, D. D. Awschalom, R. A. Buhrman, J. M. Daughton, S. von Molnar, M. L. Roukes, A. Y. Chtchelkanova, and D. M. Treger, *Science* **294**, 1488 (2001).

<sup>3</sup>S. Das Sarma, *Am. Sci.* **89**, 516 (2001).

<sup>4</sup>D. D. Awschalom, M. E. Flatte, and N. Samarth, *Sci. Am. Int. Ed.* **286**, 66 (2002).

<sup>5</sup>I. Zutic, *J. Supercond.* **15**, 5 (2002).

<sup>6</sup>S. Datta and B. Das, *Appl. Phys. Lett.* **56**, 665 (1990).

- <sup>7</sup>B. E. Kane, L. N. Pfeiffer, and K. W. West, *Phys. Rev. B* **46**, 7264 1992 .
- <sup>8</sup>M. Johnson, *Science* **260**, 320 1993 .
- <sup>9</sup>M. E. Flatte and G. Vignale, *Appl. Phys. Lett.* **78**, 1273 2001 .
- <sup>10</sup>I. Zutic, J. Fabian, and S. Das Sarma, *Appl. Phys. Lett.* **79**, 1558 2001 .
- <sup>11</sup>C. Ciuti, J. P. McGuire, and L. J. Sham, *Appl. Phys. Lett.* **81**, 4781 2002 .
- <sup>12</sup>T. Koga, J. Nitta, and H. Takayanagi, *Phys. Rev. Lett.* **88**, 126601 2002 .
- <sup>13</sup>X. F. Wang, P. Vasilopoulos, and F. M. Peeters, *Phys. Rev. B* **65**, 165217 2002 .
- <sup>14</sup>R. G. Mani, W. B. Johnson, V. Narayanamurti, V. Privman, and Y.-H. Zhang, *Physica E Amsterdam* **12**, 152 2002 .
- <sup>15</sup>S. F. Alvarado and P. Renaud, *Phys. Rev. Lett.* **68**, 1387 1992 .
- <sup>16</sup>J. Kikkawa and D. D. Awschalom, *Science* **277**, 1284 1997 .
- <sup>17</sup>M. Oestreich, J. Hubner, D. Hagele, P. J. Klar, W. Heimbrodt, W. W. Ruhle, D. E. Ashenford, and B. Lunn, *Appl. Phys. Lett.* **74**, 1251 1999 .
- <sup>18</sup>Y. Ohno, D. K. Young, B. Beschoten, F. Matsukura, H. Ohno, and D. D. Awschalom, *Nature London* **402**, 790 1999 .
- <sup>19</sup>G. Schmidt, D. Ferrand, L. W. Molenkamp, A. T. Filip, and B. J. van Wees, *Phys. Rev. B* **62**, R4790 2000 .
- <sup>20</sup>G. Schmidt, C. Gould, P. Grabs, A. M. Lunde, G. Richter, A. Slobodskyy, and L. W. Molenkamp, Preprint cond-mat/0206347 at [www.arxiv.org](http://www.arxiv.org) 2002 .
- <sup>21</sup>A. T. Filip, B. H. Hoving, F. J. Jedema, B. J. van Wees, B. Dutta, and S. Borghs, *Phys. Rev. B* **62**, 9996 2000 .
- <sup>22</sup>K. H. Ploog, *J. Appl. Phys.* **91**, 7256 2002 .
- <sup>23</sup>P. R. Hammar and M. Johnson, *Phys. Rev. Lett.* **88**, 066806 2002 .
- <sup>24</sup>A. T. Hanbicki, B. T. Jonker, G. Itkos, G. Kioseoglou, and A. Petrou, *Appl. Phys. Lett.* **80**, 1240 2002 .
- <sup>25</sup>R. Fiederling, M. Keim, G. Reuscher, W. Ossau, G. Schmidt, A. Waag, and L. W. Molenkamp, *Nature London* **402**, 787 1999 .
- <sup>26</sup>B. T. Jonker, Y. D. Park, B. R. Bennett, H. D. Cheong, G. Kioseoglou, and A. Petrou, *Phys. Rev. B* **62**, 8180 2000 .
- <sup>27</sup>K. C. Hall, S. W. Leonard, H. M. van Driel, A. R. Kost, E. Selvig, and D. H. Chow, *Appl. Phys. Lett.* **75**, 4156 1999 .
- <sup>28</sup>Y. Ohno, R. Terauchi, T. Adachi, F. Matsukura, and H. Ohno, *Phys. Rev. Lett.* **83**, 4196 1999 .
- <sup>29</sup>A. Tackeuchi, T. Kuroda, Sh. Muto, and O. Wada, *Physica B* **272**, 318 1999 .
- <sup>30</sup>A. Malinowski, R. S. Britton, T. Grevatt, R. T. Harley, D. A. Ritchie, and M. Y. Simmons, *Phys. Rev. B* **62**, 13034 2000 .
- <sup>31</sup>T. Adachi, Y. Ohno, R. Terauchi, F. Matsukura, and H. Ohno, *Physica E Amsterdam* **7**, 1015 2000 .
- <sup>32</sup>M. I. Dyakonov and V. Yu. Kachorovskii, *Sov. Phys. Semicond.* **20**, 110 1986 .
- <sup>33</sup>A. Fert and I. A. Campbell, *J. Phys. Paris, Colloq.* **32**, C1 1971 .
- <sup>34</sup>B. Das, D. C. Miller, S. Datta, R. Reifenberger, W. P. Hong, P. K. Bhattacharya, J. Singh, and M. Jaffe, *Phys. Rev. B* **39**, 1411 1989 .
- <sup>35</sup>J. Nitta, T. Akazaki, and H. Takayanagi, *Phys. Rev. Lett.* **78**, 1335 1997 .
- <sup>36</sup>P. D. Dresselhaus, C. M. A. Papavassiliou, R. G. Wheeler, and R. N. Sacks, *Phys. Rev. Lett.* **68**, 106 1992 .
- <sup>37</sup>W. Knap, C. Skierbiszewski, A. Zduniak, E. Litwin-Staszewska, D. Bertho, F. Kobbi, J. L. Robert, G. E. Pikus, F. G. Pikus, S. V. Iordanskii, V. Mosser, K. Zekentes, and Yu. B. Lyanda-Geller, *Phys. Rev. B* **53**, 3912 1996 .
- <sup>38</sup>T. Koga, J. Nitta, T. Akazaki, and H. Takayanagi, *Phys. Rev. Lett.* **89**, 046801 2002 .
- <sup>39</sup>Y. Sato, T. Kita, S. Gozu, and S. Yamada, *Physica E Amsterdam* **12**, 399 2002 .
- <sup>40</sup>D. Hagele, M. Oestreich, W. W. Ruhle, N. Nestle, and K. Eberl, *Appl. Phys. Lett.* **73**, 1580 1998 .
- <sup>41</sup>H. Sanada, I. Arata, Y. Ohno, Z. Chen, K. Kayanuma, Y. Oka, F. Matsukura, and H. Ohno, *Appl. Phys. Lett.* **81**, 2788 2002 .
- <sup>42</sup>L. Geppert, *IEEE Spectrum* **39**, 28 Issue 10, October, 2002 .
- <sup>43</sup>F. Mireles and G. Kirczenow, *Phys. Rev. B* **64**, 024426 2001 .
- <sup>44</sup>Th. Schapers, J. Nitta, H. B. Heersche, and H. Takayanagi, *Physica E Amsterdam* **13**, 564 2002 .
- <sup>45</sup>J. Fabian, I. Zutic, and S. Das Sarma, *Phys. Rev. B* **66**, 165301 2002 .
- <sup>46</sup>G. Schmidt and L. W. Molenkamp, *Semicond. Sci. Technol.* **17**, 310 2002 .
- <sup>47</sup>Z. G. Yu and M. E. Flatte, *Phys. Rev. B* **66**, 235302 2002 .
- <sup>48</sup>J. Inoue, G. E. W. Bauer, and L. W. Molenkamp, *Phys. Rev. B* **67**, 033104 2003 .
- <sup>49</sup>I. Zutic, J. Fabian, and S. Das Sarma, *Phys. Rev. Lett.* **88**, 066603 2002 .
- <sup>50</sup>T. Valet and A. Fert, *Phys. Rev. B* **48**, 7099 1993 .
- <sup>51</sup>M. Q. Weng and M. W. Wu, *J. Appl. Phys.* **93**, 410 2003 .
- <sup>52</sup>Y. Qi and S. Zhang, *Phys. Rev. B* **67**, 052407 2003 .
- <sup>53</sup>W. H. Lau, J. T. Olesberg, and M. E. Flatte, *Phys. Rev. B* **64**, 161301 2001 .
- <sup>54</sup>I. I. Puller, L. G. Mourokh, N. J. M. Horing, and A. Yu. Smirnov, *Phys. Rev. B* **67**, 155309 2003 .
- <sup>55</sup>M.-C. Cheng, *J. Phys. D* **32**, 3047 1999 .
- <sup>56</sup>N. S. Averkiev, L. E. Golub, and M. Willander, *J. Phys.: Condens. Matter* **14**, R271 2002 .
- <sup>57</sup>A. Bournel, P. Dollfus, S. Galdin, F.-X. Musalem, and P. Hesto, *Solid State Commun.* **104**, 85 1997 .
- <sup>58</sup>A. Bournel, V. Delmouly, P. Dollfus, G. Tremblay, and P. Hesto, *Physica E Amsterdam* **10**, 86 2001 .
- <sup>59</sup>A. A. Kiselev and K. W. Kim, *Phys. Rev. B* **61**, 13115 2000 .
- <sup>60</sup>K. Tomizawa, *Numerical Simulation of Submicron Semiconductor Devices* Artech House, London, Boston, 1993 .
- <sup>61</sup>C. Moglestue, *Monte Carlo Simulation of Semiconductor Devices* Chapman and Hall, London, 1993 .
- <sup>62</sup>V. V. Mitin, V. A. Kochelap, and M. A. Stroschio, *Quantum Heterostructures. Microelectronics and Optoelectronics* Cambridge University Press, Cambridge, U.K., 1999 .
- <sup>63</sup>G. Dresselhaus, *Phys. Rev.* **100**, 580 1955 .
- <sup>64</sup>Yu. Bychkov and E. I. Rashba, *J. Phys. C* **17**, 6039 1984 .
- <sup>65</sup>R. J. Elliott, *Phys. Rev.* **96**, 266 1954 .
- <sup>66</sup>M. V. Fischetti and S. E. Laux, *DAMOCLES Theoretical Manual* IBM, Yorktown Heights, 1995 .
- <sup>67</sup>M. Shen, S. Saikin, M.-C. Cheng, and V. Privman, *Lect. Notes Comp. Sci.* **2668**, 881 2003 .
- <sup>68</sup>K. Blum, *Density Matrix Theory and Applications* Plenum, New York, 1996 .
- <sup>69</sup>M. Cardona, N. E. Christensen, and G. Fasol, *Phys. Rev. B* **38**, 1806 1988 .
- <sup>70</sup>A. Tackeuchi, O. Wada, and Y. Nishikawa, *Appl. Phys. Lett.* **70**, 1131 1997 .
- <sup>71</sup>E. A. de Andrada e Silva, G. C. La Rocca, and F. Bassani, *Phys. Rev. B* **50**, 8523 1994 .
- <sup>72</sup>M. Cahay and S. Bandyopadhyay, Preprint cond-mat/0301052 at [www.arxiv.org](http://www.arxiv.org) 2003 .